Engineering 6 (2020) 644–652

Contents lists available at ScienceDirect

Engineering

journal homepage: www.elsevier.com/locate/eng

Research
Materials Genome Engineering—Article

An Investigation of Creep Resistance in Grade 91 Steel through Computational Thermodynamics

Andrew Smith [a], Mohammad Asadikiya [a,b], Mei Yang [b], Jiuhua Chen [a], Yu Zhong [a,b,*]

[a] Department of Mechanical and Materials Engineering, Florida International University, Miami, FL 33174, USA
[b] Mechanical Engineering Department, Worcester Polytechnic Institute, Worcester, MA 01609, USA

ARTICLE INFO

Article history:
Received 9 August 2018
Revised 13 April 2019
Accepted 28 June 2019
Available online 11 December 2019

Keywords:
Grade 91 steel
Creep resistance
Ferritic–martensitic steels
Welding microstructure
Computational thermodynamics
Secondary phase
Alloy composition

ABSTRACT

This study was conducted to understand the relationship between various critical temperatures and the stability of the secondary phases inside the heat-affected-zone (HAZ) of welded Grade 91 (Gr.91) steel parts. Type IV cracking has been observed in the HAZ, and it is widely accepted that the stabilities of the secondary phases in Gr.91 steel are critical to the creep resistance, which is related to the crack failure of this steel. In this work, the stabilities of the secondary phases, including those of the $M_{23}C_6$, MX, and Z phases, were simulated by computational thermodynamics. Equilibrium cooling and Scheil simulations were carried out in order to understand the phase stability in welded Gr.91 steel. The effect of four critical temperatures—that is, Ac1 (the threshold temperature at which austenite begins to form), Ac3 (the threshold temperature at which ferrite is fully transformed into austenite), and the $M_{23}C_6$ and Z phase threshold temperatures—on the thickness of the HAZ and phase stability in the HAZ is discussed. Overall, the simulations presented in this paper explain the mechanisms that can affect the creep resistance of Gr.91 steel, and can offer a possible solution to the problem of how to increase creep resistance at elevated temperatures by optimizing the steel composition, welding, and heat treatment process parameters. The simulation results from this work provide guidance for future alloy development to improve creep resistance in order to prevent type IV cracking.

1. Introduction

Grade 91 (Gr.91) steel is a high-chromium (Cr) ferritic–martensitic structural steel that was originally produced by Oak Ridge National Laboratory in the 1970s, and that has been extensively utilized by the power industries, most notably for thick-section boiler components [1]. This alloy steel has high creep resistance, due to the formation of fine secondary-phase $M_{23}C_6$ and MX particles in the matrix and grain boundaries. However, past studies have established that there are two possible mechanisms of premature creep failure, which cause the formation of type IV cracks along the heat-affected-zone (HAZ) that can be observed under short-term or long-term creep tests. Short-term creep tests are performed at higher temperatures and under high stresses, while long-term creep tests are optimized for longer periods of time with lower temperatures and low stresses. The first mechanism of premature creep failure is the coarsening of $M_{23}C_6$ at high temperature and high stress, which occurs during short-term creep testing [2–4]. $M_{23}C_6$ is viewed as a beneficial phase in the initial microstructure, due to its fine particle size. However, volume percentage increase and particle size coarsening of $M_{23}C_6$ are typically observed during or after heat treatment, changing $M_{23}C_6$ into a secondary phase that is detrimental for creep resistance. The second mechanism is the precipitation of the detrimental Z phase; this occurs under the low temperature and low stress of long-term tests [3,5–7], and "eats" away the fine MX particles.

Decades of research on the issue of creep failure in Gr.91 steel have involved extensive thermodynamic, kinetic, and crystallographic investigations, most of which have focused on direct simulations of creep failure [3,8,9]. However, very few fundamental investigations have been conducted on the stabilities of the critical secondary phases, which are directly linked to the creep resistance of this steel, even though computational thermodynamics is widely accepted as an extremely useful means of providing predictions and guidance for the design of new alloys—and especially of steels. To address this issue, a thermodynamic investigation of Gr.91 steel was carried out in order to examine the relationship

* Corresponding author.
E-mail address: yzhong@wpi.edu (Y. Zhong).

https://doi.org/10.1016/j.eng.2019.12.004

between various critical temperatures and the stabilities of the $M_{23}C_6$, MX, and Z phases within the HAZ, which can be used to predict and improve the creep resistance under both short-term and long-term applications. This investigation paves the way for a comprehensive understanding of how to optimize the alloy composition to improve the creep resistance.

2. Literature review

2.1. Type IV cracks and creep resistance in Gr.91 steel

Creep resistance degradation is considered to be the main reason for type IV cracks in welded Gr.91 steel, which occurs under repeated cyclic loading. These cracks are mostly observed to occur along the outer edge of the HAZ—more specifically, in the fine-grain HAZ (FGHAZ) and intercritical HAZ (ICHAZ) (Fig. 1), which are created by the welding process and will be explained in further detail below. Various works have been carried out in order to understand the formation mechanism of type IV cracks and to propose a method to suppress these cracks. However, the exact mechanism leading to critical failure along the HAZ is still unknown, although many suggestions have been made [10–15]. From a thermodynamic viewpoint, it has been observed that secondary phases, such as the $M_{23}C_6$, MX, and Z phases, not only change the microstructure of the HAZ, but also directly affect the alloys' failure under long-term and short-term applications. The formation and stability of secondary phases are determined by the alloy composition, welding process parameters such as the temperature gradient, and the alloy's application conditions. Therefore, thermodynamic simulations are an effective approach to investigate the formation and stability of the secondary phases, which could lead to the determination of the underlying mechanism of type IV cracks.

2.2. Microstructure of the HAZ

The HAZ is considered to be the most likely place for premature creep failure, since it has been widely observed to form type IV cracks. Three main factors affect the microstructure evolution of the HAZ and its subzones: ① the peak welding temperatures, ② the Ac1 and Ac3 temperatures (defined below), and ③ the formation and dissolution of $M_{23}C_6$ carbides [15,16]. The MX phase is not considered during the formation of the HAZ because it does not dissolve or destabilize during welding [17]. Studies have shown that its changes are much smaller, due to its high thermal stability, small coarsening, and fine distribution within the microstructure [17,18]. Therefore, the phase stability and coarsening of $M_{23}C_6$ are the primary focus in most studies on the HAZ formation.

Fig. 1 shows the schematic microstructure of the HAZ and the location of its three subzones in Gr.91 steel. After the welding process, Gr.91 steel has been observed to form three subzones within the HAZ: the coarse-grain HAZ (CGHAZ), FGHAZ, and ICHAZ. It is widely accepted that the microstructure of the HAZ is closely related to the two Ac temperatures, Ac1 and Ac3. The Ac1 temperature is defined as the temperature at which austenite begins to form, whereas the Ac3 temperature is the temperature at which austenite transformation is completed. The first zone next to the weld metal is the CGHAZ, which is located near the fusion line. In this zone, the peak temperature during welding is above Ac3, and is also higher than the $M_{23}C_6$ stability temperature region. In the CGHAZ, $M_{23}C_6$ particles on the grain boundary dissolve into the matrix, which reduces the pinning force, leading to coarsening of the grains. In the FGHAZ, which is next to the CGHAZ, the peak temperature is also above the Ac3, but lies within the $M_{23}C_6$ stability temperature region. Therefore, the $M_{23}C_6$ particles on the grain boundary cannot dissolve into the matrix. Thus, very fine grain size is observed in the FGHAZ due to the grain boundary pinning effect from $M_{23}C_6$.

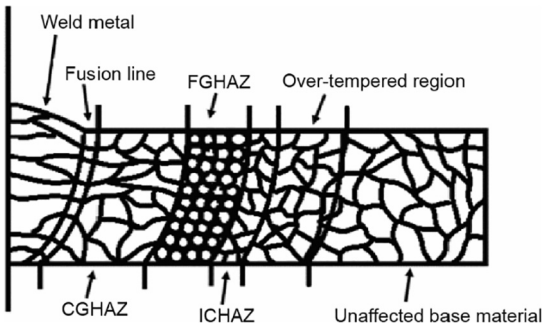

Fig. 1. Schematic microstructure of the HAZ and its three subzones formed during the welding process: the coarse-grain HAZ (CGHAZ), FGHAZ, and ICHAZ.

The ICHAZ, which is the smallest of the three zones, is located furthest from the fusion line and has a peak temperature between Ac1 and Ac3. This zone differs from the other two zones in that upon cooling, a mixture of fresh martensite and ferrite forms, whereas the CGHAZ and the FGHAZ contain mostly martensite upon cooling. Hence, from a thermodynamic perspective, the $M_{23}C_6$ stability region and the Ac temperatures are considered to be the critical factors determining the microstructure of the HAZ subzones. The Ac3 temperature determines the boundary location between the CGHAZ and FGHAZ, and the Ac1 temperature determines the boundary location between the ICHAZ and the over-tempered region.

2.3. Long-term creep failure

Long-term creep tests of Gr.91 steel are defined as tests of a material's creep life expectancy that last for 100 000 h or more, with the preferred stresses for testing being below 100 MPa [5,7,18–20]. In these tests, the testing temperature will be as low as 550 °C [5,7]. It has been observed that the Z phase will eventually form and reduce the creep resistance of the material [21]. The Z phase has been particularly studied in the last few decades, and it has been found that its formation can lead to a decrease of the fine MX carbonitrides (M(C,N)) and to the disappearance of niobium (Nb)-rich (NbX) MX phases [22,23], both of which are considered to be beneficial to the material's creep strength within the HAZ. It is believed that the formation of the Z phase within the steel determines the premature creep resistance damage during long-term operations.

2.4. Short-term creep failure

To investigate the creep resistance mechanism over a short time period, speed-up failure creep tests were designed. For example, the total creep life resulting in short-term failure can vary from 100 to 1000 h at temperatures between 575 and 650 °C [24] and under high stresses between 100 and 200 MPa, depending on the heat-treatment conditions prior to testing [3,24]. The main observation is that the increase and coarsening of $M_{23}C_6$ particles influence the microstructure in the HAZ, and can lower the creep resistance.

Many factors have been observed to affect the coarsening of $M_{23}C_6$, including the presence of creep voids in the HAZ [25–27] and neutron irradiation [28–31]. However, the mechanism of the coarsening of $M_{23}C_6$ has been best described based on the Ostwald ripening effect [20,32–35], which is considered to be the last stage of precipitation and is mainly dependent on the working

temperature of the material. Higher temperatures correspond to a higher coarsening rate of $M_{23}C_6$.

2.5. Elements pertaining to Gr.91 secondary phases

Understanding the composition of the secondary phases and the role of each element in contributing to the formation of secondary phases such as the $M_{23}C_6$, MX, and Z phases is necessary in order to study the different mechanisms of creep resistance degradation in Gr.91 steel at various operation temperatures. The typical concentration of each element and their tolerances under the American Society of Mechanical Engineers (ASME) standards [36] in the material are provided in Table 1. The "M" in $M_{23}C_6$ carbides represents the metals Cr, iron (Fe), or molybdenum (Mo), while the "M" in MX represents vanadium (V) or Nb. The "X" in MX represents carbon (C) or nitrogen (N), and has been observed to vary throughout the material, making these phases carbides (MC), nitrides (MN), or carbonitrides (M,(C,N)) [37]. The Z phase forms at lower temperatures over the long-term usage of the material [5]. Its crystal structure has three different sites—(Fe,Cr)(Mo,V,Nb)(N,Va)—where Va stands for vacancies. This paper adapts the notation of Cr(V,Nb)N for the Z phase for ease of comprehension, since the Fe and Mo concentrations are extremely low.

In general, the elements in Gr.91 steel can be grouped into two categories—ferrite (α-Fe) stabilizers and austenite (γ-Fe) stabilizers—which affect both the Ac temperatures and the stability of the secondary phases. α-Fe stabilizers are elements added to the steel alloy that have a large solubility in the α-Fe phase, thereby increasing the alloy's Ac temperatures; in contrast, γ-Fe stabilizers have a large solubility in the γ-Fe phase, thereby decreasing the Ac temperatures. C and N are both γ-Fe stabilizers [38], and are both essential to the stabilities of the MX and $M_{23}C_6$ precipitates that form and coarsen during the normalization and tempering process of the heat treatment. Cr, which is an α-Fe stabilizer [38], is the most important element in the alloy. At sufficiently large concentrations, Cr can prevent oxidation and corrosion under aqueous conditions. Cr is the essential element in the creation of the carbide $M_{23}C_6$ that makes up most of the secondary phases that form during the initial stages of heat treatment. Other precipitates also form, such as the M_7C_3 (Cr_7C_3) and M_2X (Cr_2N) precipitates, if changes are made to the composition [38,39]. Mo is an α-Fe stabilizer that provides a solid solution for the $M_{23}C_6$ ($Mo_{23}C_6$) carbides [38]. A limited amount needs to be added in order to prevent an abundance of both Laves phase $(Fe,Cr)_2(Mo,W)$ and δ-phase formation [37]. At low amounts of Cr, M_2C (Mo_2C) can form [39]. Lastly, V and Nb (which are γ-Fe stabilizers [38]) are strong suppliers to the formation of MX, especially in Gr.91 steel. MX precipitates are extremely stable even at temperatures higher than the normalization process temperature, which makes them difficult to produce but beneficial in improving the creep resistance.

3. Thermodynamic investigation

To determine the stability of the critical secondary phases in Gr.91—that is, the $M_{23}C_6$, MX, and Z phases—the calculation of phase diagrams (CALPHAD) approach based on computational thermodynamics was utilized by using Thermo-Calc and its corresponding TCFE8 database. The CALPHAD approach was first developed by Kaufman [40] to model complex multicomponent materials and their corresponding equilibrium phases. The basic concept of CALPHAD is to gather and analyze thermodynamic data from individual phases and use this data to predict the properties of materials under a wide range of temperatures, pressures, and compositional conditions [41–48].

The chemical composition of the Gr.91-based system is shown in Table 1. Here, the weight percentage of each element under ASME standards [36] is compared with the composition chosen for the current simulations. The alloy consists of more than 13 elements; however, only the most critical elements were selected in the current thermodynamic simulations, especially for the prediction of the stability of the secondary phases. Therefore, an Fe–Cr–C–V–Nb–Mo–N (Gr.91-based system) alloy was chosen as the base material for the investigation.

3.1. Isopleth diagrams of the Gr.91-based system

Fig. 2 shows the isopleth diagrams of the Gr.91-based system with changes in the carbon concentration. More specifically, Fig. 2(a) is the isopleth diagram for a C concentration ranging from 0 to 0.2 wt% at temperatures between 600 and 1600 °C, whereas Fig. 2(b) is the diagram for 0–0.15 wt% of C at 700–1000 °C. The isopleth diagrams show the phase stability region for the α and γ matrix phases along with the critical secondary phases, including the MX phase, $M_{23}C_6$ phase, and Z phase.

It is worth noting that the MX phase has the same face-centered cubic (fcc) crystal structure as the matrix γ phase. However, the Gibbs energy of the MX has a miscibility gap, which means that two fcc MX phases with different compositions can be formed within a specific temperature region. This finding agrees well with the experimental observations for this particular family of alloys [49–53]. A more detailed discussion on the Gibbs energy of the MX phases and the matrix γ phase is provided in the subsection below. The MX phase can be described as a solid solution phase with two sublattices: (V,Nb)(C,N). The first sublattice is mainly occupied with V and Nb, while C and N occupy the second sublattice. In the current work, MX1 is used to describe the MX phase, which has a higher site fraction of N than C in the second sublattice. MX2 is used to describe the phase in which the site fraction of C is higher than that of N in the second sublattice.

Detailed simulations have been done to show that the composition of the $M_{23}C_6$ phase—that is, $(Cr,Fe,Mo)_{23}C_6$—does not change much in this steel alloy; this phase has Cr as the dominant element in the first sublattice, and forms in the lower temperature region [38]. The Z phase—that is, (Fe,Cr)(Mo,V,Nb)(N,Va)—forms at even lower temperatures; its composition does not change much, and Cr and V are always the dominant elements in the first and the second sublattices, respectively [23].

At 0.05 wt% of C, the first secondary phase that is precipitated out during the temperature change from 1243 to 896 °C is the MX1 phase. When the temperature drops to the Ac3 temperature (896 °C), the γ phase starts to transform into the α phase. As the temperature decreases further, the other two secondary

Table 1
Chemical composition from the ASME standard [36] and simulation of the Gr.91-based system.

Status	Elements (wt%)												
	Cr	C	V	Nb	Mo	N	Mn	P	S	Si	Al	Ti	Zr
ASME standard	7.90–9.60	0.06–0.15	0.16–0.27	0.05–0.11	0.80–1.10	0.025–0.080	0.25–0.66	0.025 (max)	0.012 (max)	0.18–0.56	0.02 (max)	0.01 (max)	0.01 (max)
Simulation	8.75	0.10	0.215	0.08	0.95	0.05	—	—	—	—	—	—	—

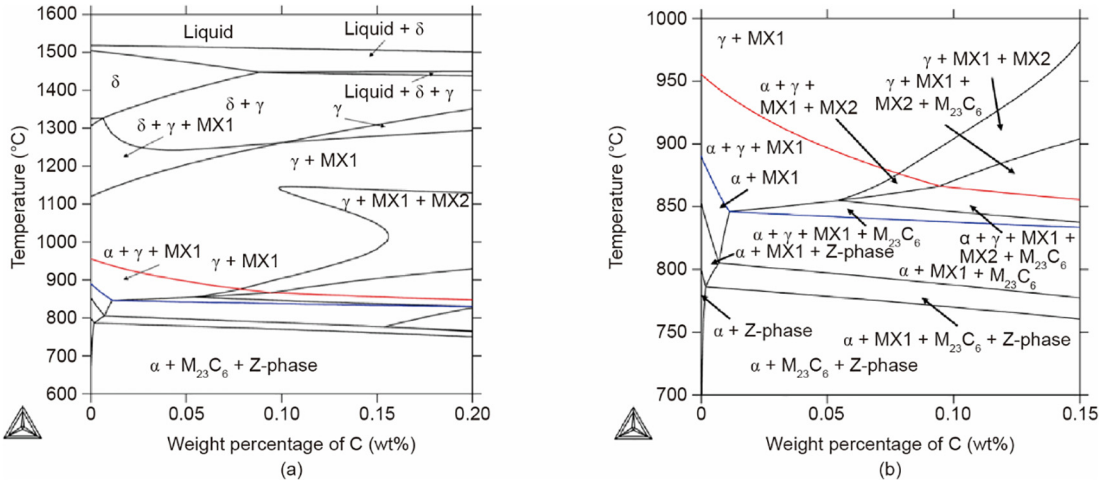

Fig. 2. Phase diagrams of the Gr.91-based system, with the Ac1 (blue) and Ac3 (red) temperatures highlighted. (a) Overall phase diagram of the Gr.91-based system for temperature ranges of 600–1600 °C at a range of 0–0.2 wt% of C; (b) close-up of the phase diagram at temperature ranges of 700–1000 °C and 0–0.15 wt% of C.

phases—that is, the $M_{23}C_6$ phase and Z phase—become stable. It should be noted that in regions with a carbon concentration higher than 0.1 wt%, two types of MX phases—MX1 and MX2—become stable due to the miscibility gap. For example, with an increase in carbon concentration, the stable phases change from γ + MX1 to γ + MX1 + MX2 around 0.155 wt% of C at 1000 °C, as shown in Fig. 2(a).

3.2. Gibbs energy of the fcc structure (γ phase and MX phase)

In the CALPHAD approach, a single Gibbs energy description is typically used to describe the phases that share the same crystal structure [23]. As mentioned above, the γ, MX1, and MX2 phases all have the fcc structure. The MX phase is considered to be beneficial for creep resistance because it is thermodynamically more stable and has a very low coarsening rate in comparison with $M_{23}C_6$ under short-term applications [38]. Therefore, it is worthwhile to take a closer look at this phase. Fig. 3 shows the Gibbs energies of the γ, MX1, and MX2 phases at 1000 °C. It can be seen that the Gibbs energies of these three phases are very different, even though the phases share the same crystal structure. In the region with less than 0.15 wt% of C, γ and MX1 are the only stable phases, while MX2 becomes stable in the region with a higher C concentration. This result clearly explains the phase transformation shown at 1000 °C in Fig. 2(a).

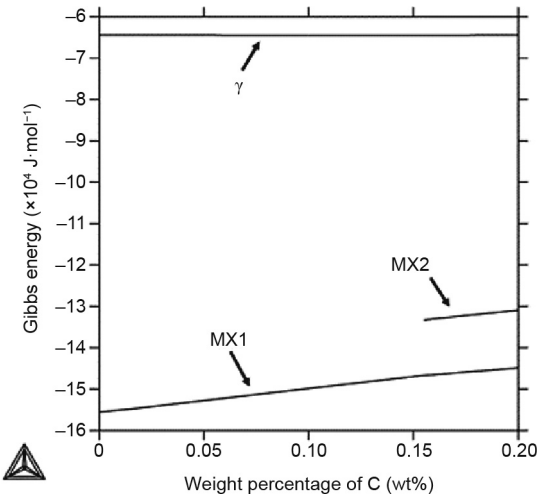

Fig. 3. Gibbs energy of the γ, MX1, and MX2 phases in the Gr.91-based system at 1000 °C from 0 to 0.20 wt% of C.

3.3. Ac1 minimum austenite transformation temperature and Ac3 threshold ferrite temperature

The two Ac temperatures—Ac1 and Ac3—are critical in understanding the phase stabilities and the microstructure evolution in the HAZ. In particular, the Ac3 temperature determines the boundary between the FGHAZ and ICHAZ, and the Ac1 temperature determines the boundary between the ICHAZ and the over-tempered region, as discussed above (Fig. 1). Therefore, these two Ac temperatures are closely linked with the formation of type IV cracks, making it worthwhile to investigate the factors that affect them. Fig. 4 shows the change of the Ac1 and Ac3 temperatures in the Gr.91-based system (solid lines) in comparison with a Fe–C binary system (dashed lines).

With an increase in the carbon concentration, as shown in Fig. 4(a), the Ac1 temperature of the Gr.91-based system drops from 890 to 830 °C, with the biggest difference happening in the beginning, up to 0.01 wt% of C, and then gradually decreasing afterwards. Similar behavior is seen for the Fe–C binary system; however, the sudden change happens at a slightly higher carbon concentration and drops from 910 to 738 °C. This sudden change in both systems is due to the phase transformation. The Ac1 temperature from the Gr.91-based system is generally much higher than that from the Fe–C system. This major difference indicates that the alloying elements in Gr.91 greatly increase the Ac1 temperature. Fig. 4(b) shows the Ac3 temperature vs. the carbon concentration. The temperature drops from 954 °C for 0 wt% of C to 850 °C for 0.2 wt% of C for the Gr.91-based system, whereas it drops from 910 to 837 °C for the Fe–C system. Similar to Fig. 4(a), the slope change in the curve for the Gr.91-based system at around 0.08 wt% of C represents a phase transformation from α + γ + MX1 + MX2 + $M_{23}C_6$ to α + γ + MX1 + $M_{23}C_6$. A linear relationship is observed for the Fe–C binary system, because there is no phase transformation—that is, α and γ are the only two stable phases in this temperature range. Overall, these findings show that Gr.91 shares similar Ac3 temperatures with the Fe–C binary system in the typical C concentration range for Gr.91—that is, for about 0.1 wt% of C.

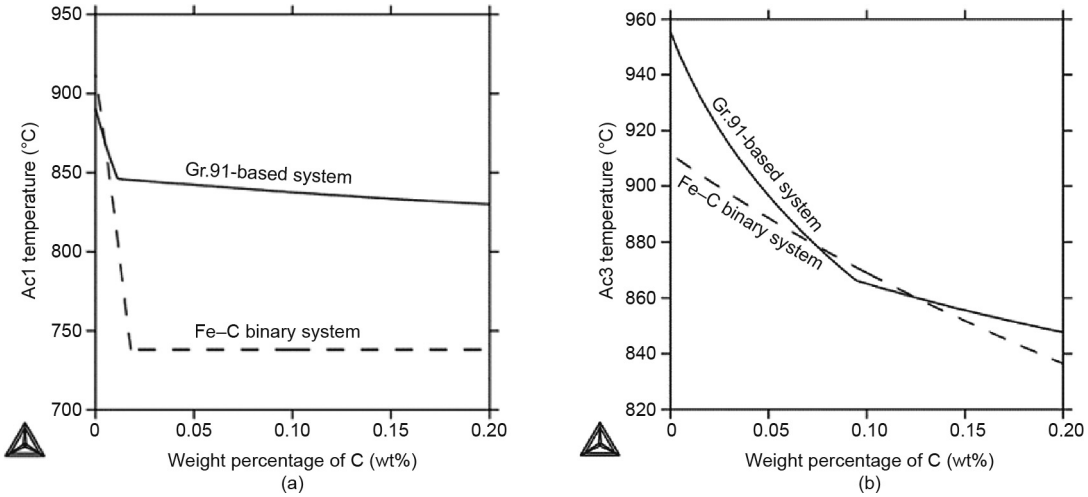

Fig. 4. (a) Ac1 and (b) Ac3 temperatures (°C) vs. weight percentage of C for the Gr.91-based system simulation (solid line) in comparison with the Ac temperatures of the Fe–C binary system (dashed line).

3.4. Mole/site fraction of secondary phases under the equilibrium condition

Fig. 5 shows the mole fraction of the secondary phases—that is, the $M_{23}C_6$, MX, and Z phases—in the temperature range between 600 and 1400 °C for the Gr.91-based steel. It can be seen that the MX1 phase is stable between 770 and 1260 °C, while a very limited amount of the fcc MX2 phase shows up briefly between 847 and 890 °C. Fig. 6 shows the changes in the site fraction in the first and second sublattices for the MX1 and MX2 phases. For MX1, it shows that the dominant species in the first sublattice changes from Nb to V with the decrease in temperature, while N is always the dominant species in the second sublattice. For the MX2 phase, Nb is always the dominant species for the first sublattice, while C has a slightly higher site fraction than N in the second sublattice. Therefore, V is an important element in MX1 at lower temperatures.

$M_{23}C_6$ becomes stable when the temperature is lower than 870 °C, and quickly becomes the dominant secondary phase with a decrease in temperature. Its dramatic concentration increase is due to the γ to α matrix phase transformation in that temperature range, which corresponds to the sudden carbon solubility decrease in the matrix.

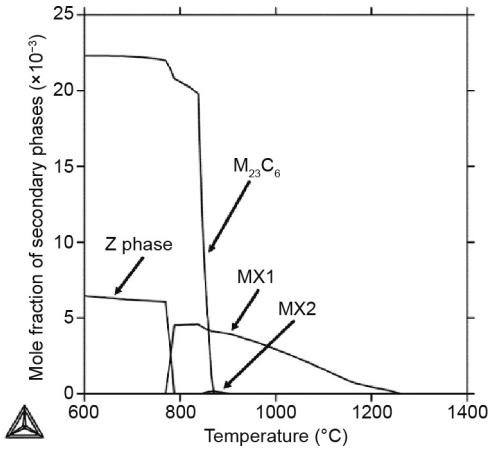

Fig. 5. Mole fraction of the secondary phases in the Gr.91-based system.

Fig. 5 also shows that the Z phase is stable at temperatures below 790 °C, when MX1 becomes unstable. The formation of the Z phase takes V from the MX1 phase and causes the decomposition of the MX1 phase. This likely to be the reason why it has been experimentally observed that the Z phase "eats" away the MX phase during low-temperature long-term creep tests [54].

3.5. Equilibrium cooling and Scheil simulations

The above equilibrium cooling simulation can be used to understand the phase stability change during the ideal slow cooling. However, a real sample does not always reach equilibrium at each temperature under typical cooling conditions. Therefore, both equilibrium cooling and Scheil simulations were carried out in order to obtain a basic understanding of the phase stabilities under real cooling conditions.

The equilibrium simulation, shown in Fig. 5, predicts the formation of secondary phases under equilibrium cooling conditions—that is, the sample reaches global equilibrium at each temperature. It is used to simulate the phase stabilities for an extremely slow cooling rate. Meanwhile, the Scheil simulation predicts the formation of secondary phases under conditions similar to the quench condition. There are three major assumptions for Scheil simulations: ① No diffusion occurs in solid phases once they are formed; ② the liquid phase is homogeneous all the time; and ③ the local equilibrium exists at the interface of the liquid and solid phases. It has been widely accepted that the equilibrium cooling and Scheil simulations can be adopted as the two boundary conditions. In other words, equilibrium cooling corresponds to an extremely slow cooling rate, while the Scheil simulation corresponds to a quenching process. Therefore, the quantity of the solid phases under real conditions should fall between what is predicted by the equilibrium cooling and Scheil simulations. In addition, using these two simulations may provide guidance regarding phase stability changes under various processing conditions, such as normalization, tempering, welding, and post-welding heat treatment. Under these conditions, the phase stability of the system will change toward the equilibrium condition as the time increases.

Fig. 7 shows the formation of the secondary phases—the $M_{23}C_6$, MX1, Z, and MX2 phases—during the solidification process of the Gr.91-based steel from the equilibrium cooling (solid line) and Scheil (dashed line) simulations. As shown in Fig. 7(a), the $M_{23}C_6$ phase precipitates out at 870 °C under equilibrium cooling

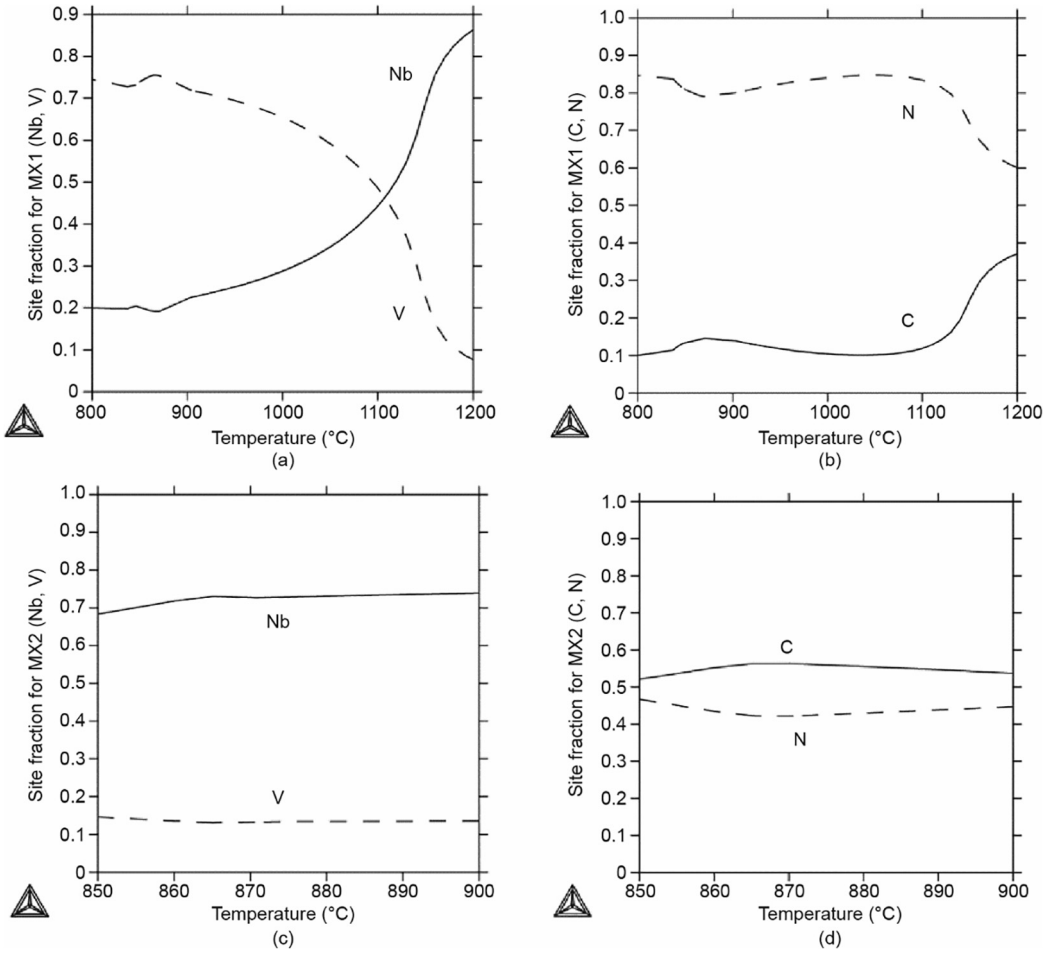

Fig. 6. Site fraction of Nb, V, C, and N (a,b) the MX1 and (c,d) the MX2 phases of the Gr.91-based system.

conditions, but forms at 1225 °C during the Scheil simulation. In addition, much less of the $M_{23}C_6$ phase will form during the Scheil simulation than during equilibrium cooling. This result indicates that the concentration of the $M_{23}C_6$ phase formed during the real cooling process may be less than that formed during the equilibrium simulations. Therefore, Gr.91 steel has a tendency to form much more of the $M_{23}C_6$ phase under annealing/operation conditions at elevated temperatures. This finding explains very well why much more of the $M_{23}C_6$ phase has been observed in Gr.91 samples under high-temperature short-term creep testing conditions [24].

On the other hand, the MX1 phase will form at 1260 °C during equilibrium cooling, as shown in Fig. 7(b), but will disappear at temperatures below 770 °C. Under fast cooling conditions, the MX1 phase will form at 1410 °C; however, its maximum content is much lower than that resulting from equilibrium cooling. This finding indicates that the observed MX phase is a metastable phase at typical operation temperatures, that its formation is due to the fast cooling speed, and that it has a tendency to disappear under high-temperature short-term creep testing conditions. The observations in Figs. 7(a) and (b) explain very well the increased molar volume of the $M_{23}C_6$ phase and the disappearance of the MX phase under high-temperature short-term creep test conditions [3].

Furthermore, Fig. 7(c) shows that the Z phase is a stable phase under equilibrium cooling conditions, and its formation temperature is lower than those of the $M_{23}C_6$ and MX phases. However, the Z phase does not form during the Scheil simulation, indicating that formation of the Z phase is prohibited by the fast cooling rate. This finding explains very well why the Z phase is not observed in the initial microstructure, and why it gradually shows up and eats away the MX phase under low-temperature long-term creep test conditions [54]. For the MX2 phase, only a small fraction forms during equilibrium simulations in a short temperature range, as shown in Fig. 2(b) and Fig. 5, while the MX2 phase is not stable at all during the Scheil simulations. Its stability will greatly depend on the cooling rate and alloy compositions.

3.6. Alloy composition effects on creep resistance

Based on the systematic thermodynamic simulations, it was found that the stabilities of various secondary phases are imperative to the creep resistance of Gr.91 alloys. The simulation results also show that the alloy composition affects the stabilities of the secondary phases. To improve the creep resistance of Gr.91 alloys, the alloy composition needs to be optimized in order to obtain the desired microstructure in the HAZ after the welding process.

As shown in Fig. 8, there are four different critical temperatures for Gr.91 alloys. Ac1 (the blue line) is the boundary between the ICHAZ and the over-tempered region, while Ac3 (the red line) is the boundary between the FGHAZ and the ICHAZ during welding. The $M_{23}C_6$ threshold temperature (the black solid line) is defined as the maximum temperature at which $M_{23}C_6$ is thermodynamically stable. In welded alloys, this corresponds to the boundary between the FGHAZ and the CGHAZ. As mentioned above, type IV cracks only occur inside the FGHAZ and ICHAZ [55]. Many suggestions have been made to explain why it is possible for type IV cracks to be located within this region of the material [3,15];

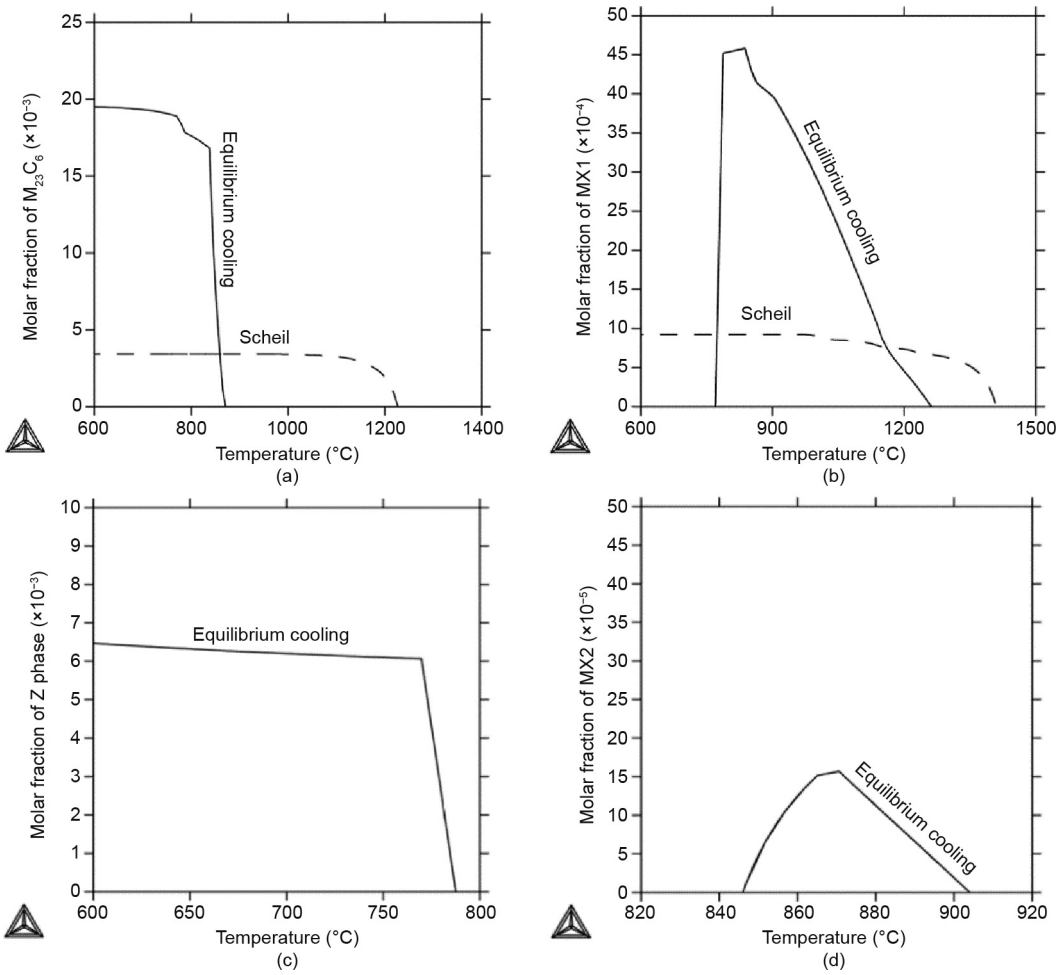

Fig. 7. Results of the equilibrium cooling (solid line) and Scheil (dashed line) simulations for the Gr.91-based system. Molar fractions for (a) the $M_{23}C_6$ phase, (b) the MX1 phase, (c) the Z phase, and (d) the MX2 phase. The Z phase and MX2 phase were not stable during the Scheil simulations.

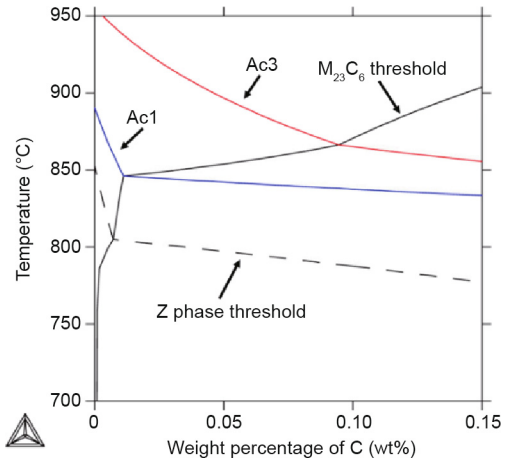

Fig. 8. Gr.91 $M_{23}C_6$ (black solid line) and Z phase (dashed line) threshold diagram, along with the Ac1 (blue solid line) and Ac3 (red solid line) temperatures.

however, from a thermodynamic point of view, two secondary phases—$M_{23}C_6$ coarsening and Z phase formation—have been observed and theorized to decrease the creep resistance between the FGHAZ and the ICHAZ [20,23,56].

Assuming that the temperature gradient inside the HAZ during the welding process is not changing, adjusting the Ac1, Ac3, and $M_{23}C_6$ threshold temperature will have a large impact on the thickness of the FGHAZ and ICHAZ. To reduce the whole thickness of the FGHAZ and ICHAZ, it is necessary to reduce the temperature difference between the Ac1 and $M_{23}C_6$ threshold temperatures. As shown in Fig. 8, reducing the carbon concentration of Gr.91 should be helpful in reducing the chance of type IV cracking.

High-temperature short-term creep resistance is related to the coarsening of the $M_{23}C_6$ phase [20,32–35]. Therefore, the creep resistance can be improved by reducing the thermodynamic stability of $M_{23}C_6$. Based on Fig. 8, the $M_{23}C_6$ threshold temperature will greatly decrease with a decrease in carbon concentration, which will decrease the stability of the $M_{23}C_6$ at high temperatures and thereby increase the high-temperature short-term creep resistance.

Low-temperature long-term creep resistance is related to the formation of the detrimental Z phase. Based on previous observations, the N-rich MX phase will eventually disappear through Cr diffusion from the grain matrix into MX, eventually transforming the MX phase into the Z phase [23]. From this observation, the assumption is that by reducing the Z phase threshold temperature, which is the maximum temperature at which the Z phase is thermodynamically stable, it should be possible to greatly improve the long-term creep resistance. As illustrated in Fig. 8, a higher carbon concentration will be helpful in improving the short-term creep resistance.

Similar thermodynamic simulations could be performed for the alloying elements, in order to investigate the effects of alloy composition on creep resistance. The approach used in the current work paves the way for the alloy composition optimization of Gr.91 in order to improve the creep resistance of this alloy under various applications.

4. Summary and future work

This work establishes a fundamental thermodynamic understanding using the CALPHAD approach by analyzing and simulating the relationship among the Ac temperatures, $M_{23}C_6$, and Z phase threshold temperatures, and stability and compositional change of the $M_{23}C_6$, MX, and Z phases in the HAZ of Gr.91 steel.

Two different thermodynamic creep mechanisms under different application conditions contributing to a decrease in creep resistance and, eventually, type IV cracks in the HAZ were discussed: ① $M_{23}C_6$ coarsening under low stress and high temperatures for short-term testing conditions through the Ostwald ripening effect [20,32–35]; and ② Z phase formation under high stress and low temperatures for long-term application conditions, which eventually decreases the overall MX phase stability within Gr.91 [22,23].

Equilibrium cooling and Scheil simulations were carried out to show the phase stabilities under two extreme cooling conditions—that is, extremely slow cooling and quench conditions. The Scheil simulations showed the formation of a limited amount of the $M_{23}C_6$ and MX1 phases under fast cooling conditions and above 1200 °C. In comparison, the equilibrium cooling simulations indicated that much more of the $M_{23}C_6$ and Z phases form at low temperatures. Meanwhile, the MX phase is thermodynamically unstable and may disappear at operation temperatures. This finding successfully explains the experimental observations of the formation of more $M_{23}C_6$, the formation of the Z phase, and the disappearance of the MX phase under creep test conditions.

In addition, effort was initiated to investigate the elements' effects on creep resistance by using carbon as a case study. To be specific, the effect of carbon on the four critical temperatures—that is, Ac1, Ac3, the $M_{23}C_6$ threshold temperature, and the MX threshold temperature—was investigated. The findings show that the addition of carbon may have various effects on the microstructure and phase stabilities. It may increase the overall thickness of the FGHAZ and ICHAZ during the welding process, which in turn may increase the likelihood of type IV cracking. Furthermore, the addition of carbon may increase the stability of $M_{23}C_6$ and decrease the stability of the Z phase, which may be detrimental to the short-term creep resistance but beneficial to the long-term creep resistance. However, based on the thermodynamic model of the secondary phases—that is, the $M_{23}C_6$ and Z phases—in Gr.91, it cannot be concluded that there is a specific carbon concentration that can change the overall stability of the secondary phases. The model highlights the overall trend of the threshold phase stability, while the mechanical properties can be altered depending on the welding conditions, which can in turn affect the HAZ microstructure. Therefore, the alloy composition needs to be optimized through both specific heat treatment conditions and creep experiments. In addition, similar simulations can reveal the role of various alloying elements in type IV cracking in the HAZ and in the creep resistance of Gr.91 steel, and will be carried out in future studies.

Acknowledgements

This material is based upon work supported by the US Department of Energy (DOE) (DE-FE0027800). The authors would like to thank the DOE National Energy Technology Laboratory program managers, Dr. Karol Schrems and Dr. Jessica Mullen, and Dr. Wei Zhang from Ohio State University, for their support and guidance.

Disclaimer

Compliance with ethics guidelines

Andrew Smith, Mohammad Asadikiya, Mei Yang, Jiuhua Chen, and Yu Zhong declare that they have no conflict of interest or financial conflicts to disclose.

References

[1] Abe F, Okada H, Wanikawa S, Tabuchi M, Itagaki T, Kimura K, et al. Guiding principles for development of advanced ferritic steels for 650 °C USC boilers. In: Proceedings of the Seventh Liege Conference on Materials for Advanced Power Engineering; 2002 Sep 30–Oct 2; Liege, Belgium; 2002. p. 1397–406.
[2] Bhadeshia HKDH. Design of ferritic creep-resistant steels. ISIJ Int 2001;41(6):626–40.
[3] Abson DJ, Rothwell JS. Review of type IV cracking of weldments in 9–12%Cr creep strength enhanced ferritic steels. Int Mater Rev 2013;58(8):437–73.
[4] Abe F. Coarsening behavior of lath and its effect on creep rates in tempered martensitic 9Cr–W steels. Mater Sci Eng A 2004;387–389:565–9.
[5] Sawada K, Kushima H, Kimura K, Tabuchi M. Z-phase formation and its effect on long-term creep strength in 9–12%Cr creep resistant steels. Trans Indian Inst Met 2010;63(2–3):117–22.
[6] Hald J. Materials for advanced power engineering. In: Proceedings of the Eighth Liege Conference on Materials for Advanced Power Engineering; 2006 Sep 18–20; Liege, Belgium; 2006.
[7] Kimura K, Sawada K, Kushima H, Toda Y. Influence of chemical composition and heat treatment on long-term creep strength of Grade 91 steel. Procedia Eng 2013;55:2–9.
[8] Abd El-Azim ME, Nasreldin AM, Zies G, Klenk A. Microstructural instability of a welded joint in P91 steel during creep at 600 °C. Mater Sci Technol 2005;21(7):779–90.
[9] Abe F, Taneike M, Sawada K. Alloy design of creep resistant 9Cr steel using a dispersion of nano-sized carbonitrides. Int J Press Vessels Piping 2007;84(1–2):3–12.
[10] Gooch DJ, Kimmins ST. A study of type IV cracking in 1/2% CrMoV/2 1/4% CrMo weldments. In: Proceedings of the Third International Conference on Creep and Fracture of Engineering Materials and Structures; 1987 Apr 5–10; Swansea, UK; 1987. p. 698–703.
[11] Kimmins ST, Coleman MC, Smith DJ. An overview of creep failure associated with heat affected zones of ferritic weldments. In: Proceedings of the Fifth International Conference on Creep and Fracture of Engineering Materials and Structures; 1993 Mar 28–Apr 2; Swansea, UK; 1993. p. 681–94.
[12] Kimmins ST, Smith DJ. On the relaxation of interface stresses during creep of ferritic steel weldments. J Strain Anal Eng Des 1998;33(3):195–206.
[13] Ellis FV, Viswanathan R. Review of type IV cracking in piping welds. In: Proceedings of the International Conference on Integrity of High Temperature Welds; 1998 Nov 3–4; London, UK; 1998.
[14] Nishimura N, Iwamoto K, Yamauchi M, Masuyama F, Imamoto T, Yokoyama T. Development of life assessment system for high energy piping in fossil power boilers. In: Proceedings of the 4th International Conference on Reliability, Maintainability and Safety; 1999 May 18; Shanghai, China; 1999. p. 347–52.
[15] Francis JA, Mazur W, Bhadeshia HKDH. Review type IV cracking in ferritic power plant steels. Mater Sci Technol 2006;22(12):1387–95.
[16] Mannan SL, Laha K. Creep behavior of Cr–Mo steel weldments. Trans Indian Inst Met 1996;49(4):303–20.
[17] Yu X, Babu SS, Terasaki H, Komizo Y, Yamamoto Y, Santella ML. Correlation of precipitate stability to increased creep resistance of Cr–Mo steel welds. Acta Mater 2013;61(6):2194–206.

[18] Chen RP, Ghassemi Armaki H, Maruyama K, Igarashi M. Long-term microstructural degradation and creep strength in Gr.91 steel. Mater Sci Eng A 2011;528(13–14):4390–4.
[19] Brinkman CR, Sikka VK, Horak JA, Santella ML. Long-term creep rupture behavior of modified 9Cr–1Mo steel base and weldment behavior. Oak Ridge TN: Oak Ridge National Laboratory; 1987. Report No.: ORNL/TM-10504.
[20] Hald J. Microstructure and long-term creep properties of 9–12% Cr steels. Int J Press Vessels Piping 2008;85(1–2):30–7.
[21] Danielsen HK, Hald J. Behaviour of Z phase in 9–12% Cr steels. Energy Mater 2006;1(1):49–57.
[22] Suzuki K, Kumai S, Kushima H, Kimura K, Abe F. Precipitation of Z-phase and precipitation sequence during creep deformation of mod. 9Cr–1Mo steel. Tetsu to Hagane 2003;89(6):691–8.
[23] Danielsen HK. Z-phase in 9–12% Cr steels [dissertation]. Lyngby: Technical University of Denmark; 2007.
[24] Cerri E, Evangelista E, Spigarelli S, Bianchi P. Evolution of microstructure in a modified 9Cr–1Mo steel during short term creep. Mater Sci Eng A 1998;245(2):285–92.
[25] Smith DJ, Walker NS, Kimmins ST. Type IV creep cavity accumulation and failure in steel welds. Int J Press Vessels Piping 2003;80(9):617–27.
[26] Lee JS, Maruyama K, Nonaka I, Ito T. Mechanism of type IV failure in weldment of a mod 9Cr–1Mo steel. In: Proceedings of the Creep Deformation and Fracture, Design and Life Extension; 2005 Sep 25–28; Pittsburgh, PA, USA; 2005. p. 139–48.
[27] Francis JA, Mazur W, Bhadeshia HKDH. Estimation of type IV cracking tendency in power plant steels. ISIJ Int 2004;44(11):1966–8.
[28] Maziasz PJ, Klueh RL, Vitek JM. Helium effects on void formation in 9Cr–1MoVNb and 12Cr–1MoVW irradiated in HFIR. J Nucl Mater 1986;141–143:929–37.
[29] Klueh RL, Kai JJ, Alexander DJ. Microstructure-mechanical properties correlation of irradiated conventional and reduced-activation martensitic steels. J Nucl Mater 1995;225:175–86.
[30] Little EA, Stoter LP. 11th conference on "effects of radiation on materials". Philadelphia: ASTM STP; 1982.
[31] Gelles DS, Thomas LE. Ferritic alloys for use in nuclear energy technologies. Warrendale: TMS-AIME; 1984.
[32] Orlova A, Buršík J, Kuchařová K, Sklenička V. Microstructural stability of creep resistant alloys for high temperature plant applications. London: The Institute of Materials; 1998.
[33] Laha K, Chandravathi KS, Parameswaran P, Bhanu Sankara Rao K, Mannan SL. Characterization of microstructures across the heat-affected zone of the modified 9Cr–1Mo weld joint to understand its role in promoting type IV cracking. Metall Mater Trans A 2007;38(1):58–68.
[34] Danielsen HK, Hald J. A thermodynamic model of the Z-phase Cr(V,Nb)N. Calphad 2007;31(4):505–14.
[35] Abe F. Analysis of creep rates of tempered martensitic 9%Cr steel based on microstructure evolution. Mater Sci Eng A 2009;510–511:64–9.
[36] Parker JD, Coleman K, Henry J, Liu W, Zhou G. Guidelines and specifications for high-reliability fossil power plants: best practice guideline for manufacturing and construction of Grade 91 steel components 1023199. California: Electric Power Research Institute; 2011. Report No.: 3002006390.
[37] Foldyna V, Kubon Z, Vodarek V, Purmensky J. How to improve creep rupture strength of advanced chromium steels. In: Proceedings of the Thrid International Conference on Advances in Materials Technology for Fossil Power Plants; 2001 Apr 5–6; Llandysul, UK; 2001.
[38] Klueh RL. Elevated temperature ferritic and martensitic steels and their application to future nuclear reactors. Int Mater Rev 2013;50(5):287–310.
[39] Viswanathan R, Nutting J. Advanced heat resistant steel for power generation. London: Institute of Materials; 1999.
[40] Zhong Y, Ozturk K, Sofo JO, Liu Z. Contribution of first-principles energetics to the Ca–Mg thermodynamic modeling. J Alloys Compd 2006;420(1–2):98–106.
[41] Asadikiya M, Rudolf C, Zhang C, Boesl B, Agarwal A, Zhong Y. Thermodynamic modeling and investigation of the oxygen effect on the sintering of B_4C. J Alloys Compd 2017;699:1022–9.
[42] Asadikiya M, Zhong Y. Oxygen ion mobility and conductivity prediction in cubic yttria-stabilized zirconia single crystals. J Mater Sci 2018;53(3):1699–709.
[43] Costa e Silva A. Applications of multicomponent databases to the improvement of steel processing and design. J Phase Equilibria Diffus 2017;38(6):916–27.
[44] Bale CW, Bélisle E, Chartrand P, Decterov SA, Eriksson G, Hack K, et al. FactSage thermochemical software and databases—recent developments. Calphad 2009;33(2):295–311.
[45] Andersson JO, Helander T, Höglund L, Shi P, Sundman B. Computational tools for materials science. Calphad 2002;26(2):273–312.
[46] Kroupa A. Modelling of phase diagrams and thermodynamic properties using Calphad method—development of thermodynamic databases. Comput Mater Sci 2013;66:3–13.
[47] Perrut M. Thermodynamic modeling by the Calphad method and its applications to innovative materials. Aerospace Lab 2015;9:1–11.
[48] Smith A, Asadikiya M, Zhong Y. The thermodynamic evaluation and modeling of Grade 91 alloy and its secondary phases through the CALPHAD approach. In: Proceedings of the 2017 Annual Review Meeting for Crosscutting Research MS&T; 2017 Mar 20–23; Pittsburgh, PA, USA; 2017.
[49] Fedorova I, Kostka A, Tkachev E, Belyakov A, Kaibyshev R. Tempering behavior of a low nitrogen boron-added 9%Cr steel. Mater Sci Eng A 2016;662:443–55.
[50] Kipelova AY, Belyakov AN, Skorobogatykh VN, Shchenkova IA, Kaibyshev RO. Tempering-induced structural changes in steel 10Kh9K3V1M1FBR and their effect on the mechanical properties. Metal Sci Heat Treat 2010;52(3–4):100–10.
[51] Kipelova A, Kaibyshev R, Belyakov A, Molodov D. Microstructure evolution in a 3%Co modified P911 heat resistant steel under tempering and creep conditions. Mater Sci Eng A 2011;528(3):1280–6.
[52] Fedoseeva A, Dudova N, Kaibyshev R. Creep strength breakdown and microstructure evolution in a 3%Co modified P92 steel. Mater Sci Eng A 2016;654:1–12.
[53] Dudova N, Plotnikova A, Molodov D, Belyakov A, Kaibyshev R. Structural changes of tempered martensitic 9%Cr–2%W–3%Co steel during creep at 650 °C. Mater Sci Eng A 2012;534:632–9.
[54] Cipolla L, Danielsen HK, Venditti D, Di Nunzio PE, Hald J, Somers MAJ. Conversion of MX nitrides to Z-phase in a martensitic 12% Cr steel. Acta Mater 2010;58(2):669–79.
[55] Laha K, Chandravathi KS, Parameswaran P, Rao KBS. Type IV cracking susceptibility in weld joints of different grades of Cr–Mo ferritic steel. Metall Mater Trans A 2009;40(2):386–97.
[56] Sawada K, Tabuchi M, Hongo H, Watanabe T, Kimura K. Z-phase formation in welded joints of high chromium ferritic steels after long-term creep. Mater Charact 2008;59(9):1161–7.